Journal of Applied Mathematics and Mechanics

ZAMM

Zeitschrift für Angewandte Mathematik und Mechanik
Founded by Richard von Mises in 1921

Edited in cooperation with Martin-Luther-Universität Halle-Wittenberg and Gesellschaft für Angewandte Mathematik und Mechanik e. V. (GAMM)

www.zamm-journal.org

ZAMM · Z. Angew. Math. Mech. **91**, No. 2, 110 – 124 (2011) / **DOI** 10.1002/zamm.201000140

Dynamic stress and electric field concentration in a functionally graded piezoelectric solid with a circular hole

Petia Dineva[1], **Dietmar Gross**[2], **Ralf Müller**[3], **and Tsviatko Rangelov**[4,*]

[1] Institute of Mechanics, Bulgarian Academy of Sciences, 1113 Sofia, Bulgaria
[2] Division of Solid Mechanics, Technische Universität Darmstadt, 64289 Darmstadt, Germany
[3] Chair of Applied Mechanics, Department of Mechanical and Process Engineering, Technische Universität Kaiserslautern, 67663 Kaiserslautern, Germany
[4] Institute of Mathematics and Informatics, Bulgarian Academy of Sciences, 1113 Sofia, Bulgaria

Received 27 July 2010, revised and accepted 25 October 2010
Published online 28 December 2010

Key words Anti-plane deformation, circular hole, functionally graded piezoelectric solid, time-harmonic electro-mechanical load, BIEM, SCF.

Dedicated to Professor Peter Wriggers on the occasion of his 60th birthday.

This work addresses the evaluation of the stress and electric field concentrations around a circular hole in a functionally graded piezoelectric plane subjected to anti-plane elastic SH-wave and in-plane time-harmonic electric load. All material parameters vary exponentially along a line of arbitrary orientation in the plane of the piezoelectric material under consideration. The computational tool is a non-hypersingular traction based boundary integral equation method (BIEM). The kernel functions used in the BIEM are exact fundamental solutions that have been derived in previous work by the authors.

Numerical solutions for the stress and electric field concentration factors (SCF and EFCF, respectively) around the perimeter of the hole are obtained. The simulation demonstrates the efficiency of the computational approach and its potential to reveal in an adequate way the dynamic stress and electric field distribution around the hole. Presented are results showing their dependence on various system parameters as e.g. the electro-mechanical coupling, the type of the dynamic load and its characteristics, the wave-hole and wave-material interaction and the magnitude and direction of the material inhomogeneity.

1 Introduction

Functional graded piezoelectric materials (FGPM) are the next generation of high performance multifunctional materials. Their structural integrity is becoming increasingly important as their use is extended to new frontiers. Due to their intrinsic electro-mechanical coupling, piezoelectrics are widely used in intelligent and advanced structures with integrated self-monitoring and online control capabilities. The structural integrity of FGPM subjected to different type of mechanical and electrical stresses in service can fail due to defects such as cracks, holes, inclusions, sharp corners, joints, delamination and porosity, arising during their manufacture. These defects present regions of high stress and electric field concentrations and may initiate a sudden mechanical failure or dielectric breakdown. Therefore, it is of great interest to study the electromechanical behaviour of piezoelectric solid with defects. It is a well known fact that brittle failure originates very often from stress concentration areas around holes. Thus, a great deal of research has been conducted to determine stress concentration factors in solids with holes. The first stress concentration study around a circular hole in an infinite elastic isotropic homogeneous plane under uniaxial static stress was done by Kirsch [20] which has been followed by many similar investigations, see Savin [38]. Corresponding dynamic stress concentration studies around circular holes were done later, see Kupradze [22], Eringen and Suhubi [12], Miklowicz [29], Baron and Matthews [3, 5], Baron and Parnes [4], Pao [33], Lee and Trifunac [24], Pao and Mow [34], Kundu and Bostrom [21], Liu and Han [25], Manolis [28]. As far as the subject of this study are FGPMs, we will restrict the short overview mainly to piezoelectric materials (PEM).

Analytical solutions for static problems of piezoelectric solids with defects have been presented in Deeg [8], Sosa [41], Pak [31, 32], Chung and Ting [6], Sosa and Khutoryansky [42]. The problem of piezoelectric solid with an elliptic cavity is

* Corresponding author E-mail: rangelov@math.bas.bg, Phone: +359 (0) 2979 2845, Fax: +359 (0) 2971 3649

considered in Sosa and Khutoryansky [42]. A circular and elliptic piezoelectric inclusion embedded in an infinite piezoelectric matrix is analyzed in Pak [31] and Pak [32], where a closed form solution is obtained for the anti-plane case. Various authors have solved the static anti-plane piezoelectric elliptic inclusion problem, see Chung and Ting [6], Jiang et al. [19], Meguid and Zhong [30]. A general static solution is provided in Sosa [41] in terms of complex potentials, with emphasis being placed on stress concentrations in the vicinity of circular and elliptical holes. The interactions of electro-elastic fields with voids and cracks contained in a piezoelectric solid under static load are addressed both in closed form and numerically in Perez-Aparicio et al. [35]. In the work by Wang [44] a solution was developed for an infinite, piezoelectric medium containing a piezoelectric ellipsoidal inclusion. In Shindo et al. [39] the dynamic theory of linear anti-plane piezoelectricity is applied to investigate the scattering of horizontally polarized shear waves by a circular piezoelectric inclusion in an infinite piezoelectric matrix subjected to an in-plane electric load. More recently, Fang et al. [13–15] studied the dynamic stresses induced by a circular cavity in a semi-infinite functionally graded material. In specific, in Fang [15] the electro-elastic field and dynamic stress around a cavity embedded in a graded piezoelectric layer bonded to a homogeneous piezoelectric substrate are investigated by analytical methods. Generally, the most used analytical and semi-analytical methods for stress concentration factor calculations are the wave function expansion, matched asymptotic expansion, integral transforms and singular integral equation methods. However, the application of analytical methods for the analysis of piezoelectric solids with defects suffers from a number of drawbacks. The most important is the inflexibility since by analytical methods only a very restricted class of problems can be treated (e.g. an elliptic void/inclusion with an axis parallel to the polarization, infinite domains, single void/inclusion homogeneous materials, etc.). A review of the literature reveals that there is a lack of numerical studies of piezoelectric problems allowing more complex mechanical, geometrical, physical, and loadings properties.

It is well known that among numerical methods the BIEM has many advantages for problems which are discussed here. However, due to the lack of fundamental solutions for anisotropic, coupled and inhomogeneous solids, the BIEM results in the field are very scarce. Lee [23], Xu and Rajapakse [46], and Liu and Fan [26] applied the BIEM to treat the static problem for a homogeneous piezoelectric solid with a hole. The paper of Xu and Rajapakse [46] considers coupled elastic and electric fields in piezoelectric solids with different types of defects. The stress concentration induced by the existence of multiple holes, cracks and inclusions and their mutual interactions was studied by Hwu and Liao [18].

Most of the references discussed above are for the static problems and for homogeneous piezoelectrics, see [6, 26, 32, 35, 42, 46]. There is still a lack of results for dynamic problems [27, 40, 41] and more specifically for dynamic problems of functionally graded piezoelectric solids [15] with holes. The present work aims to contribute to the gap's closing by studying numerically the stress and electric field distribution around a hole in an inhomogeneous piezoelectric plane under incident SH-wave and in-plane time-harmonic electrical loading. The analysis is an extension of previous results of the authors, see Rangelov et al. [36] and Dineva et al. [11], where the anti-plane and in-plane crack problem in functionally graded piezoelectric solids have been analyzed by using the BIEM. For this purpose the authors derived fundamental solutions in closed form for certain classes of smoothly inhomogeneous piezoelectric materials of quadratic, exponential and sinusoidal type.

The paper is organized as follows: the problem statement is given in Sect. 2. The non-hypersingular traction based BIE formulation of the problem is presented in Sect. 3. The numerical solution procedure and a series of results, including their interpretation, are discussed in Sect. 4, while some conclusions are drawn in Sect. 5.

2 Basic equations

2.1 Anti-plane deformation

Consider an infinite transversely isotropic functionally graded piezoelectric material with its axis of symmetry and poling axis both along the x_3 axis of an Cartesian coordinate system $Ox_1x_2x_3$. A single circular hole H of radius c and center $(0,0)$ is embedded in the plane $x_3 = 0$. The mechanical load is given by (shear) SH waves with a circular frequency ω, polarized in Ox_3 direction and propagating in the plane $x_3 = 0$ under the incident angle θ with respect to the x_1 axis, see Fig. 1. Additionally, an in-plane electric load with the same frequency ω may be applied. The only non-vanishing displacements are the anti-plane mechanical displacement $u_3(\mathbf{x}, t)$ and the in-plane electrical displacements $D_j(\mathbf{x}, t)$, $j = 1, 2$, $\mathbf{x} = (x_1, x_2)$. In this case the field equations in absence of body forces consist of the constitutive equations

$$\begin{aligned} \sigma_{13} &= c_{44}s_{13} - e_{15}E_1, \\ \sigma_{23} &= c_{44}s_{23} - e_{15}E_2, \\ D_1 &= e_{15}s_{13} + \varepsilon_{11}E_1, \\ D_2 &= e_{15}s_{23} + \varepsilon_{11}E_2, \end{aligned} \tag{1}$$

the strain-displacement and electric field-potential relations

$$s_{i3} = u_{3,i}, \quad E_i = -\Phi_{,i}, \tag{2}$$

and the balance equations

$$\sigma_{i3,i} = \rho u_{3,tt}, \quad D_{i,i} = 0. \tag{3}$$

Here σ_{i3}, s_{i3}, E_i, ϕ are the stress tensor, strain tensor, electric field vector, and electric potential, respectively, where $i = 1, 2$. Subscript commas denote partial differentiation and the summation convention over repeated indices is invoked. Since we assume that the mass density ρ, the shear stiffness c_{44}, the piezoelectric e_{15} and the dielectric permittivity ε_{11} vary in arbitrary direction α in the plane $x_3 = 0$, the field equations must be regarded as a system with non-constant coefficients.

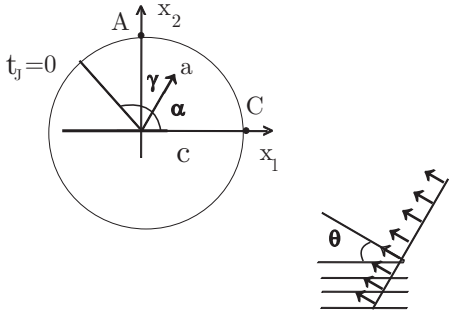

Fig. 1 A hole with radius c in a piezoelectric plane with direction of material inhomogeneity α subjected to incident plane SH wave with incident angle θ. The location of the observer point is defined by angle γ.

By introducing the notation of the generalized displacement $u_J = (u_3, \Phi)$, $J = 3, 4$, the field equations may be written in the compact form

$$\sigma_{iJ,i} = \rho_{JK} u_{K,tt}, \quad J, K = 3, 4, \tag{4}$$

where

$$\rho_{JK} = \begin{cases} \rho, \, J = K = 3, \\ 0, \, J = 4 \text{ or } K = 4, \end{cases} \quad \sigma_{iJ} = \begin{cases} \sigma_{ij}, \, J = 3, \\ D_i, \, J = 4, \end{cases} \quad \sigma_{iJ} = C_{iJKl} u_{K,l},$$
$$C_{i33l} = \begin{cases} c_{44}, \, i = l, \\ 0, \quad i \neq l, \end{cases} \quad C_{i34l} = \begin{cases} e_{15}, \, i = l, \\ 0, \quad i \neq l, \end{cases} \quad C_{i44l} = \begin{cases} -\varepsilon_{11}, \, i = l, \\ 0, \quad\quad i \neq l. \end{cases} \tag{5}$$

The interaction of an incident wave with the hole induces scattered waves. The total wave field at a given field point can be written as the sum of the incident (in) and the scattered (sc) wave field which both must fulfill the wave equation (4): $u_J = u_J^{in} + u_J^{sc}$, $\sigma_{iJ} = \sigma_{iJ}^{in} + \sigma_{iJ}^{sc}$. The boundary condition along the boundary S of the hole is

$$t_J|_S = 0, \tag{6}$$

where the total generalized traction is expressed by Cauchy's formula $t_J = \sigma_{iJ} n_i$, with $\mathbf{n} = (n_1, n_2)$ being the outward normal to S. The condition (6) implies that the boundary of the hole is free of mechanical traction as well as of surface charges, i.e. the hole is electrically impermeable. In the case of a circular hole in a piezoelectric material this assumption is reasonable [31].

2.2 The type and characteristics of material inhomogeneity

In the following we assume that the mass density ρ and material parameters C_{iJKl} vary in the same manner exponentially with vector position $\mathbf{x}$. Thus, introducing the function $h(\mathbf{x}) = \mathrm{e}^{2\langle \mathbf{a}, \mathbf{x} \rangle}$, where $\langle ., . \rangle$ denotes the scalar product in R^2 i.e. $\langle \mathbf{a}, \mathbf{x} \rangle = (a_1 x_1 + a_2 x_2)$, the parameters can be written as

$$c_{44}(\mathbf{x}) = c_{44}^0 h(\mathbf{x}), \quad e_{15}(\mathbf{x}) = e_{15}^0 h(\mathbf{x}), \quad \varepsilon_{11}(\mathbf{x}) = \varepsilon_{11}^0 h(\mathbf{x}), \quad \rho(\mathbf{x}) = \rho^0 h(\mathbf{x}), \tag{7}$$

and correspondingly $C_{iJKl}(\mathbf{x}) = C_{iJKl}^0 h(\mathbf{x})$. Here the material constants c_{44}^0, e_{15}^0, ε_{11}^0, and ρ^0 are the reference constants, i.e. the material characteristics in the homogeneous case. The inhomogeneity parameter, the vector **a** can be written in polar

coordinates as $\mathbf{a} = r(\cos\alpha, \sin\alpha)$, where α and $r = \sqrt{a_1^2 + a_2^2}$ are the direction and the magnitude of the inhomogeneity gradient. Note that for $\mathbf{a} = 0$, i.e. $h = 1$, the material is homogeneous.

We will study the time-harmonic solutions $u_J(\mathbf{x}, \omega)$ of the BVP (4), (6). Therefore, suppressing in the following the common multiplier $\mathrm{e}^{i\omega t}$, Eq. (4) becomes

$$\sigma_{iJ,i} + \rho_{JK}\,\omega^2 u_K = 0, \quad J, K = 3, 4, \tag{8}$$

This equation constitutes a system of partial differential equations with variable coefficients that govern the wave propagation in a smoothly inhomogeneous piezoelectric plane. Let us introduce the smooth change of functions

$$u_J(\mathbf{x}, \omega) = \mathrm{e}^{-\langle \mathbf{a}, \mathbf{x}\rangle} U_J(\mathbf{x}, \omega). \tag{9}$$

and suppose that $U_J(\mathbf{x}, \omega)$ satisfies Sommerfeld-type condition at infinity, more specifically

$$U_3 = o(|\mathbf{x}|^{-1}), U_4 = o(\mathrm{e}^{-|\mathbf{a}||\mathbf{x}|}) \quad \text{for} \quad |\mathbf{x}| \to \infty. \tag{10}$$

Condition (10) ensures uniqueness of the scattering field u_J^{sc} for a given incident field u_J^{in}. Following Akamatsu and Nakamura [1] it can be proved that the boundary value problem (BVP) (4), (6) admits continuous differentiable solutions.

Following the approach developed in [10,28,36] for the solution of mechanical problems of functionally graded materials and applying the smooth transform (9) to (8) we obtain the following system with constant coefficients for $U_J(\mathbf{x}, \omega)$

$$C_{iJKl}^0 U_{K,il} + (\rho_{JK}^0 \omega^2 - C_{iJKi}^0 |\mathbf{a}|^2) U_K = 0. \tag{11}$$

Eliminating U_4 by inserting the second equation of (11) into the first one, the reduced wave equation

$$\Delta U_3 + k^2 U_3 = 0 \tag{12}$$

for U_3 is obtained, where $\Delta = \partial_{11}^2 + \partial_{22}^2$ is the Laplace operator and $k^2 = \omega^2 \rho^0 / a_0 - |\mathbf{a}|^2$, $a_0 = c_{44}^0 + (e_{15}^0)^2 / \varepsilon_{11}^0$. Introducing a critical frequency by $\omega_0^2 = |\mathbf{a}|^2 a_0 / \rho^0$ the following three cases with respect to the frequency ω of the applied load must be distinguished:

1. $\omega > \omega_0$, in this case $k^2 > 0$,
2. $\omega = \omega_0$, in this case $k^2 = 0$,
3. $\omega < \omega_0$, in this case $k^2 < 0$.

From the mechanical point of view the 3rd case characterizes a simple vibration while in case 2 the system behaves statically, i.e. stationary wave propagation does not occur in these cases. Only case 1 characterizes wave propagation phenomena, see [7]. Thus, the type of the dynamic behavior of exponentially inhomogeneous materials is governed by the frequency of the applied dynamic load and the inertial and electro-elastic properties of the piezoelectric material. The present study focuses on case 1 and in what follows, for fixed inhomogeneity magnitude $r = |\mathbf{a}|$, the frequency ω of the applied load is assumed to be greater than the critical frequency ω_0.

2.3 Electro-mechanical load

As already mentioned, the mechanical load is given by time harmonic SH wave propagating in the plane $x_3 = 0$ under incident angle θ with respect to the x_1 axis. The generalized displacement u_J^m and traction t_J^m fields due to this load satisfy the wave equation (8). Denoting $\eta = (\eta_1, \eta_2)$ with $\eta_1 = \cos\theta$, $\eta_2 = \sin\theta$, applying the smooth transformation to the displacement vector and using the solution of Eq. (11), the following expressions for the incident wave are obtained

$$u_3^m = \mathrm{e}^{-\langle \mathbf{x}, \mathbf{a} + ik\eta\rangle}, \qquad u_4^m = \frac{e_{15}^0}{\varepsilon_{11}^0} \mathrm{e}^{-\langle \mathbf{x}, \mathbf{a} + ik\eta\rangle}. \tag{13}$$

Here the superscript m indicates the mechanical load. The induced traction t_J^m along the boundary S of the hole is

$$t_3^m = -a_0 \langle \mathbf{a} + ik\eta, \mathbf{n}\rangle \mathrm{e}^{\langle \mathbf{x}, \mathbf{a} - ik\eta\rangle}, \qquad t_4^m = 0. \tag{14}$$

Additionally an incident time-harmonic pure electric in-plane load along S is applied which is described by

$$u_3^e = 0, \qquad \phi = -E_0 \langle \mathbf{x}, \eta\rangle. \tag{15}$$

The corresponding traction t_J^e along the boundary S of the hole is

$$t_3^e = -e_{15}^0 E_0 \langle \mathbf{n}, \eta \rangle, \qquad t_4^e = \varepsilon_{11}^0 E_0 \langle \mathbf{n}, \eta \rangle. \tag{16}$$

In the case of a homogeneous solid, i.e. $|\mathbf{a}| = 0$ and a wave with an incidence angle $\theta = 0$, formulae (13)–(16) are the same as in Shindo et al. [39]. It also should be mentioned that although the wave propagation direction θ and the inhomogeneity direction α in our case are two independent parameters, only the relative direction $\theta - \alpha$ is finally of importance. This is due to the specific type of wave loading (plane SH wave) and anisotropy (transversely isotropic). Thus, without loss of generality, the inhomogeneity direction could have been chosen as fixed in an arbitrary direction, e.g. $\alpha = 0$ leaving θ as the only free parameter. This has not been done in this investigation in view of generalizations of the method to other loading cases and types of anisotropy.

The total incident generalized displacement and traction fields are

$$u_J^{in} = u_J^m + u_J^e, \qquad t_J^{in} = t_J^m + t_J^e. \tag{17}$$

One way to solve numerically the BVP (8), (6) is to transform it into the equivalent integro-differential equation along the boundary of the hole S. This will be done by the use of the fundamental solution of the wave equation (8) within the framework of the non-hypersingular traction BIEM.

3 BIEM formulation and fundamental solution

As can be seen from the governing equation (8), the solution of wave motion problems in inhomogeneous media involves the solution of partial differential equations with variable coefficients. The key role played by the fundamental solution in a BIEM is to reduce a given BVP into a system of BIE through the usage of reciprocal theorem. The BVP formulated in Sect. 2 in this work is described by a system of non-hypersingular traction based BIEs on the boundary S of the hole. This formulation was proposed for the first time by Zhang and Gross [47] for cracked homogeneous isotropic, purely elastic infinite anti-plane solids. In a series of works (see, Gross et al. [16, 17], Dineva et al. [9], Rangelov et al. [37]) this method was developed further and applied for the solution of dynamic in-plane and anti-plane crack problems for homogeneous anisotropic piezoelectric infinite and finite solids. The same approach was used successfully to study plane fracture problems of inhomogeneous piezoelectric solids, see Rangelov et al. [36], Dineva and Rangelov [10], and Dineva et al. [11].

For u_J, u_{JK}^*, where u_{JK}^* is the fundamental solution of (4), we apply the Green's formula in the domain $\Omega_R \setminus \Omega_\varepsilon$, Ω_R is a circular domain with large radius R and Ω_ε is a small neighborhood of the hole. Applying the representation formulae for the generalized displacement gradient $u_{K,l}$, see [45] an integro-differential equation on $\partial\Omega_R \cup \partial\Omega_\varepsilon$ is obtained. Using the condition (10) integrals over $\partial\Omega_R$ go to 0 for $R \to \infty$. Taking the limit $\varepsilon \to 0$, i.e. $x \to S$ and using the boundary condition (6), i.e. $t_J^{sc} = -t_J^{in}$ on S, the following system of non-hypersingular traction BIE describes the posed problem:

$$\begin{aligned} -\frac{1}{2} t_J^{in}(\mathbf{x}) = C_{iJKl}(\mathbf{x}) n_i(\mathbf{x}) \int_S [(\sigma_{\eta PK}^*(\mathbf{x}, \mathbf{y}, \omega) u_{P,\eta}(\mathbf{y}, \omega) - \rho_{QP}\omega^2 u_{QK}^*(\mathbf{x}, \mathbf{y}, \omega) u_P(\mathbf{y}, \omega)) \delta_{\lambda l} \\ -\sigma_{\lambda PK}^*(\mathbf{x}, \mathbf{y}, \omega) u_{P,l}(\mathbf{y}, \omega)] n_\lambda(\mathbf{y}) dS - C_{iJKl}(\mathbf{x}) n_i(\mathbf{x}) \int_S u_{PK,l}^*(\mathbf{x}, \mathbf{y}, \omega) t_P^{in}(\mathbf{y}, \omega) dS, \quad \mathbf{x} \in S. \end{aligned} \tag{18}$$

Here, u_{QK}^* is the fundamental solution of (8) and $\sigma_{iJQ}^* = C_{iJKl} u_{KQ,l}^*$ is the corresponding stress. Furthermore, $\mathbf{x}$ and $\mathbf{y}$ denote the position vector of the observation point and source point, respectively. Eq. (18) constitutes a system of integro-differential equations for the unknown generalized displacements u_J on the boundary S of the hole. From this solution, the generalized displacement u_J and traction t_J of the scattered wave field at each point in the inhomogeneous piezoelectric domain $R^2 \setminus H$ can be determined by using the corresponding representation formulae. These solutions, for example, can be used in the field of nondestructive evaluation of materials.

In order to solve the system (18) it is necessary to know the fundamental solutions for displacement and traction and their derivatives. The fundamental solution of (8) is defined as solution of the equation

$$\sigma_{iJM,i}^* + \rho_{JK}\omega^2 u_{KM}^* = -\delta_{JM}\delta(\mathbf{x}, \xi), \tag{19}$$

where $\mathbf{x} = (x_1, x_2)$, $\xi = (\xi_1, \xi_2)$, δ is Dirac's function and δ_{JM} is the Kronecker symbol. The fundamental solution was derived in Rangelov et al. [36] and is shortly given here for the sake of completeness of the description.

First with a suitable transformation of the displacement vector, Eq. (19) is transformed into an equation with constant coefficients. The second step is to apply the Radon transform and to obtain a system of ordinary differential equations. This

system of differential equations is decoupled via linear algebra tools. The third step is to apply the inverse Radon transform and to find the fundamental solution. In the first step the smooth transformation

$$u^*_{KM} = h^{-1/2} U^*_{KM} \tag{20}$$

applied to (19) gives (compare Sect. 2.2)

$$C^0_{iJKi} U^*_{KM,ii} + [\rho^0_{JK}\omega^2 - C^0_{iJKi} a_i^2] U^*_{KM} = h^{-1/2}(\xi)\delta_{JM}\delta(x,\xi). \tag{21}$$

To solve Eq. (21) we use the Radon transform, see Zayed [48]. In R^2 it is defined for the set $f \in \Im$ of rapidly decreasing C^∞ functions as $\hat{f}(s,m) = R[f(x)] = \int_{\langle m,x\rangle = s} f(x)dx = \int f(x)\delta(s - \langle m,x\rangle)dx$ with the inverse transform $f(x) = \frac{1}{4\pi^2}\int_{|m|=1} K(\hat{f}(s,m)|_{s=\langle m,x\rangle} dm$, $K(\hat{f}) = \int_{-\infty}^{\infty} \frac{\partial_\sigma \hat{f}(\sigma,m)}{s-\sigma} d\sigma$. Applying the Radon transform to both sides of Eq. (21) we get with $p_{JK} = C^0_{iJKi} a_i^2$

$$[C^0_{iJKi} m_i^2 \partial_s^2 + (\rho^0_{JK}\omega^2 - p_{JK})]\hat{U}^*_{KM} = -h^{-1/2}(\xi)\delta_{JM}\delta(s - \langle \xi, m\rangle). \tag{22}$$

These are two systems of two linear second order ordinary differential equations. Following Vladimirov [43], their solutions are obtained as

$$\begin{aligned} &\hat{U}^*_{33} = h^{-1/2}(\xi)\frac{i}{2ka_0}\mathrm{e}^{ik|s-\tau|}, \qquad \hat{U}^*_{34} = h^{-1/2}(\xi)\frac{i}{2ka_0}\frac{e^0_{15}}{\varepsilon^0_{11}}\mathrm{e}^{ik|s-\tau|}, \\ &\hat{U}^*_{43} = \hat{U}^*_{34}, \qquad \hat{U}^*_{44} = h^{-1/2}(\xi)\left[\frac{i}{2ka_0}\left(\frac{e^0_{15}}{\varepsilon^0_{11}}\right)^2 \mathrm{e}^{ik|s-\tau|} + \frac{1}{2\varepsilon^0_{11}|a|}\mathrm{e}^{|a|\,|\varepsilon-r|}\right]. \end{aligned} \tag{23}$$

In order to obtain the fundamental solution we finally have to apply the inverse Radon transform to $\hat{U}^*_{KJ}$. Since the functions $\hat{U}^*_{KJ}$ are linear combinations of the terms $\mathrm{e}^{iq|s-\tau|}$ and $\mathrm{e}^{q|s-\tau|}$, for the first part of the inverse Radon transform the following formulas

$$\begin{aligned} &K(\mathrm{e}^{iq|s-\tau|}) = -iq\{i\pi\mathrm{e}^{iq\beta} - 2[\mathrm{ci}(q\beta)\cos(q\beta) + \mathrm{si}(q\beta)\sin(q\beta)]\}|_{\beta=|s-\tau|}\,, \\ &K(\mathrm{e}^{q|s-\tau|}) = q\{2[\mathrm{chi}(q\beta)\cosh(q\beta) - \mathrm{shi}(q\beta)\sinh(q\beta)]\}|_{\beta=|s-\tau|} \end{aligned} \tag{24}$$

are used. Here $\mathrm{ci}(\eta) = -\int_\eta^\infty \frac{\cos t}{t} dt$, $\mathrm{si}(\eta) = -\int_\eta^\infty \frac{\sin t}{t} dt$ are the cosine integral and sine integral functions and $\mathrm{chi}(\eta) = -\int_0^\eta \frac{\cosh t - 1}{t} dt + \ln\eta + C$, $\mathrm{shi}(\eta) = -\int_0^\eta \frac{\sinh t}{t} dt$ are the hyperbolic cosine and sine integral functions with C being Euler's constant, see Bateman and Erdelyi [2].

After having obtained $\hat{U}^*_{KJ}$ by completing the inverse Radon transforms, the final form of the fundamental solution is derived by the smooth transformation (20). Using the properties of hyperbolic and trigonometric integral functions for small arguments and the properties of the function h, we obtain the asymptotic behaviour of the fundamental solution. When the field point $x \to \xi$, the continuity of the function h implies that $h(x) = h(\xi) + O(|x-\xi|)$. Thus, we get

$$\begin{aligned} &u^{*as}_{JK} = h^{-1}(\xi) U^{*as}_{JK} = h^{-1} b_{JK} \ln|x-\xi|\,, \\ &\sigma^{*as}_{iJM} = C_{iJKl} u^{*as}_{JK,l} = C^0_{iJKl}\left[-\frac{1}{2}h^{-1}(\xi)h_{,l}(\xi) b_{JK}\ln|x-\xi| + \eta_{MKl}\frac{1}{|x-\xi|}\right], \end{aligned} \tag{25}$$

where b_{JK} and η_{MKl} depend on elastic, dielectric, piezoelectric constants, and density, but not on the frequency.

To make the BIEM analysis tractable, the focus is limited on a special class of smoothly inhomogeneous materials in which material properties vary in the same proportion. This idealization results in ratios (such as wave speeds) that are macroscopically constant. The mechanical, the electrical, and piezoelectric properties of the electromechanical continuum are considered for a class of functional forms for which the fundamental solution of the considered wave equation can be derived in an efficient analytical form. In our opinion it is worth to use such an idealization because obtained solutions reveal some new effects of the material inhomogeneity and its influence on the stress and electric field concentration. Additionally these results are useful for benchmarks of more complex mechanical models and more effective computational tools.

4 Numerical results

4.1 Numerical solution procedure

The numerical treatment of the boundary-value problem consists of the following steps: (a) evaluation of the singular behavior of the fundamental solutions, their derivatives, and their near and far-field asymptotics; (b) discretization mesh preparation: the displacement and traction are approximated by parabolic shape functions; (c) evaluation of the singularities of the kernels of the integrals obtained after discretization: they are at least Cauchy principal value (CPV) integrals; (d) solution of all obtained regular and singular integrals and their validation: the regular integrals are computed employing the Gaussian quadrature scheme for one-dimensional integrals and Monte Carlo integration scheme for two-dimensional integrals where integration is done over the boundary element and over the unit circumference which is involved in the 2D fundamental solution, see Gross et al. [16]. All singular integrals and integrals with logarithmic singularity are solved analytically for a small neighborhood of the source point, using the approximation of the fundamental solution for a small argument, and numerically for the remaining part of the boundary element; (e) assembly of the system of equations and formation of the matrix of the complex algebraic system; (f) solution of the complex algebraic system of equations; (g) post processing, i.e. back substitution of the boundary solutions in order to obtain additional results: the displacement and traction of the scattered wave field, and by this the total field, can be determined in the whole domain by the corresponding representation formula. Knowing the total stress field, the generalized SCF is computed. As a result of the physical phenomena like wave diffraction and scattering, the stresses near the hole are different, in some regions essentially higher than the stresses at the same point produced by undisturbed waves, a phenomenon known as dynamic stress concentration. Following Pao and Mow [34] for the pure elastic case and Fang [15], Shindo et al. [39] for the piezoelectric case, the dynamic SCF and electric field concentration factor (EFCF) along the perimeter of a circular hole is defined as the ratio of the stress and electric field amplitude along the circumference to the maximum amplitude of the incident stress at the same point.

The normalized dynamic SCF $|\sigma_{\gamma\theta}/\tau_0|$ and the normalized dynamic EFCF $|e_{15}E_{\gamma\theta}/\tau_0|$ are calculated by using the following formulae:

$$\begin{aligned} &\sigma_{\theta\gamma} = -\sigma_1 \sin(\theta-\gamma) + \sigma_2 \cos(\theta-\gamma), \quad \sigma_i = \sigma_{i3} + \sigma_{i3}^{in}, \\ &E_{\theta\gamma} = -E_1 \sin(\theta-\gamma) + E_2 \cos(\theta-\gamma), \quad E_i = \frac{e_{15}^0}{e_{15}^{02} + c_{44}^0 \varepsilon_{11}^0}(-e_{15}^0\sigma_i + c_{44}^0 D_i), \quad D_i = \sigma_{i4} + \sigma_{i4}^{in}. \end{aligned} \tag{26}$$

Here τ_0 is the amplitude of the maximal shear stress of the incident plane SH-wave, i.e. $\tau_0 = i\omega\sqrt{a_0\rho^0}$ and a_0 is defined in Sect. 2.2, see also Fig. 1, γ is the angle of the observation point and θ is the angle of the incident wave.

For the calculations, presented in the following, meshes of 10 quadratic boundary elements have been used. In general, BIEM mesh discretization issues such as mesh density and the element size are controlled by the well-known accuracy condition $\lambda/l \geq 10$, where l is the length of a boundary element and λ is the shear wavelength.

4.2 Validation study

To the author's best knowledge there are no results available for SCF computation concerning a circular hole in an exponentially inhomogeneous piezoelectric plane subjected to time-harmonic anti-plane mechanical and in-plane electrical load. Therefore, the present non-hypersingular, traction-type BIEM and its numerical realization can only be validated by comparison with results from the literature for homogeneous materials. This easily can be done by setting the inhomogeneity function h in the developed program code to $h(\mathbf{x}) = 1$. Two examples from the literature are chosen which have been solved by using the analytical wave function expansion method. The first refers to a circular hole embedded in a homogeneous piezoelectric plane which is loaded by a mechanical SH wave, propagating in positive Ox_1 direction in conjunction with a time-harmonic electrical in-plane load $E_1 = E_0 \mathrm{e}^{-i\omega t}$ and $E_2 = 0$ [39]. The respective reference material data of lead zirconate titanate (PZT-4) piezoceramic are given in Table 1. A dimensionless frequency is introduced, defined as $\Omega = c\sqrt{\frac{\rho^0}{c_{44}^0}}\omega$. Furthermore, a parameter $E^* = E_0 \frac{e_{15}^0}{\tau_0}$ is used, where E_0 is the amplitude of the applied electrical load, to normalize appropriately the amplitude of the applied electrical field by the amplitude of the maximal shear stress of the incident SH-wave. The value of E^* is chosen to be $0.0, \pm 0.5$ and 1.0. Figs. 2 and 3 show a comparison of the results for the normalized generalized concentration field (GCF) – SCF and EFCF versus normalized frequency Ω at the observation point $A(0, c)$ for all four values of E^*. As can be seen, the BIEM results agree very well with those of Shindo et al. [39]. The difference of both results is below 7%, indicating a high accuracy of the obtained solution.

As second test example serves the solution for a circular hole in a homogeneous isotropic purely elastic plane, loaded by an incident SH-wave, propagating in Ox_1 direction [34]. The results in Fig. 4a are obtained by using the same numerical scheme and the same program code. They show the SCF at point $A(0, c)$ on account of an incident plane SH-wave with

Table 1 Reference properties of the piezoelectric material.

Material	Elastic stiffness c_{44}^0 (10^{10} N/m^2)	Piezoelectric coefficient e_{15}^0 (C/m^2)	Dielectric constant ε_{11}^0 (10^{-10} C/Vm)	Density ρ^0 (10^3 kg/m^3)
PZT-4	2.56	12.7	64.6	7.5

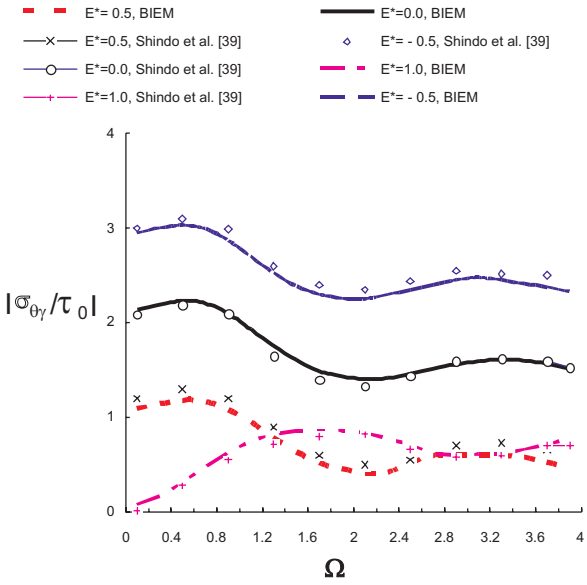

Fig. 2 (online colour at: www.zamm-journal.org) Dynamic SCF at observer point $A(0, c)$ versus normalized frequency Ω of the incident plane SH-wave with incident angle $\theta = 0$ for different electromechanical loads E^*.

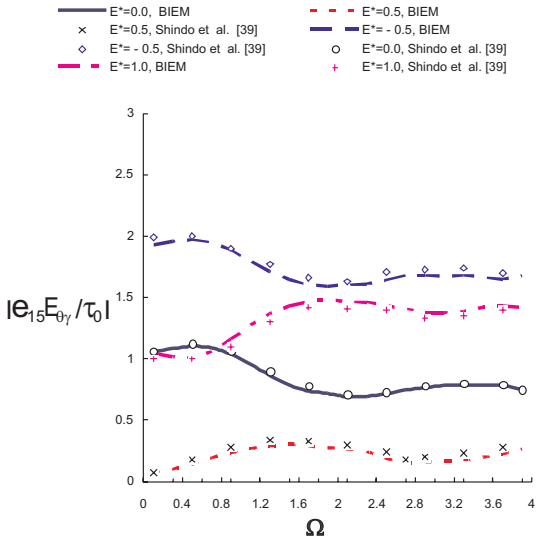

Fig. 3 (online colour at: www.zamm-journal.org) Dynamic EFCF at observer point $A(0, c)$ versus normalized frequency Ω of the incident plane SH-wave with incident angle $\theta = 0$ for different electromechanical loads E^*.

incident angle $\theta = 0^0$. It can be seen that the BIEM solutions are very close to those obtained by Pao and Mow [34]. The same results are shown in Fig. 4b, where the angular distribution of the SCF along the hole is drawn for three fixed normalized frequencies $\Omega = 0.1$, $\Omega = 1.0$, and $\Omega = 2.0$.

4.3 Simulation results

The aim of the parametric study conducted here is to show how the stress and electrical field concentration factors are influenced by some key parameters like: (a) the frequency, the wave propagation direction and the type of the electromechanical load; (b) the inherent properties of the functional graded piezoelectric materials like anisotropy and electro-mechanical coupling; (c) the location of the observer where the stress and electric field concentration is measured; (d) the magnitude and the direction of the material inhomogeneity. Note that in all figures the condition $\Omega > \Omega_0$ is satisfied where $\Omega_0 = rc$ is the critical dimensionless frequency, see Sect. 2.2.

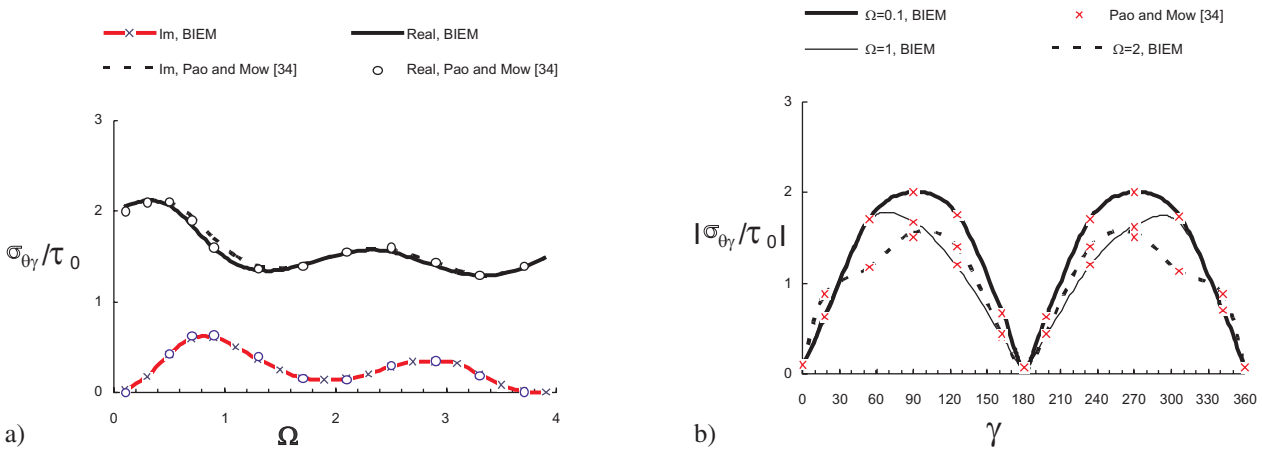

Fig. 4 (online colour at: www.zamm-journal.org) Dynamic SCF in the case of incident plane SH-wave with incident angle $\theta = 0$: (a) at observer point $\gamma = \pi/2$, i.e. $A(0, c)$ versus normalized frequency Ω; (b) for angular distribution γ at fixed frequencies Ω.

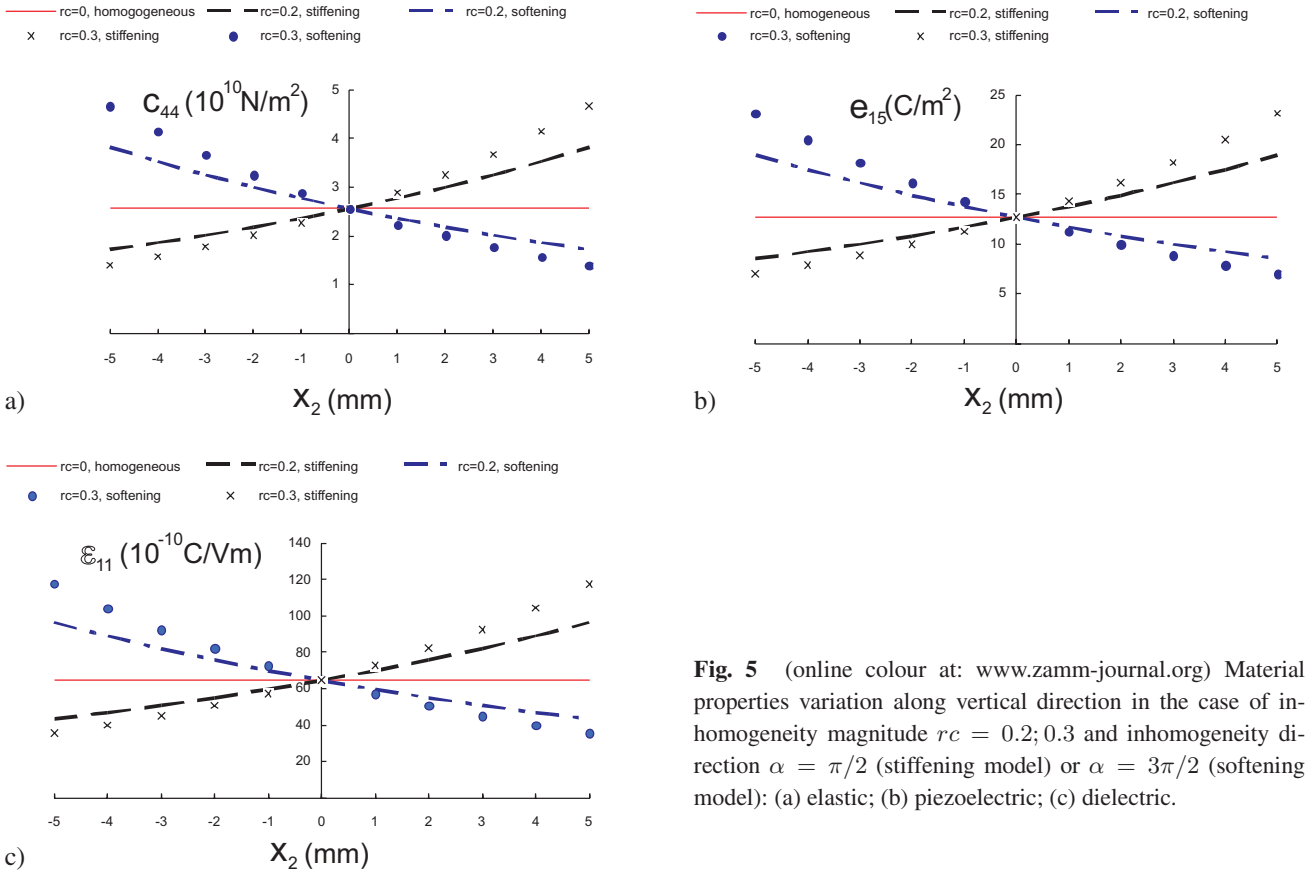

Fig. 5 (online colour at: www.zamm-journal.org) Material properties variation along vertical direction in the case of inhomogeneity magnitude $rc = 0.2; 0.3$ and inhomogeneity direction $\alpha = \pi/2$ (stiffening model) or $\alpha = 3\pi/2$ (softening model): (a) elastic; (b) piezoelectric; (c) dielectric.

The FGPM under consideration is the piezoceramic PZT-4 with the reference material properties given in Table 1. For chosen inhomogeneity directions $\alpha = \pi/2$ or $\alpha = 3\pi/2$ and a hole radius $c = 5$ mm, the variation of the material properties along the vertical x_2 axis is shown in Fig. 5 for the dimensionless inhomogeneity parameters $rc = 0.2$ and $rc = 0.3$. We consider the following specific cases: material stiffening along the Ox_1-axis when $\alpha = 0$, i.e. $a_1 > 0, a_2 = 0$, material softening along the Ox_1-axis in the case of $\alpha = \pi$, i.e. $a_1 < 0, a_2 = 0$; material stiffening along the Ox_2-axis when $\alpha = \pi/2$, i.e. $a_1 = 0, a_2 > 0$ and material softens along the Ox_2-axis when $\alpha = 3\pi/2$, i.e. $a_1 = 0, a_2 < 0$.

Figs. 6a,b present SCF and EFCF at observer points $A(0, c)$ and $C(c, 0)$ versus normalized frequency of the incident wave with incidence angle $\theta = 0$, inhomogeneity direction $\alpha = \pi/2$ or $\alpha = 3\pi/2$ (i.e. along the Ox_2-axis) and inhomogeneity parameter $rc = 0.0, 0.1, 0.2$. This is the case of pure mechanical load, i.e. $E^* = 0$. The stiffening and softening models are considered. It is first observed that the basic shape of SCF and EFCF curve in homogeneous case is preserved in

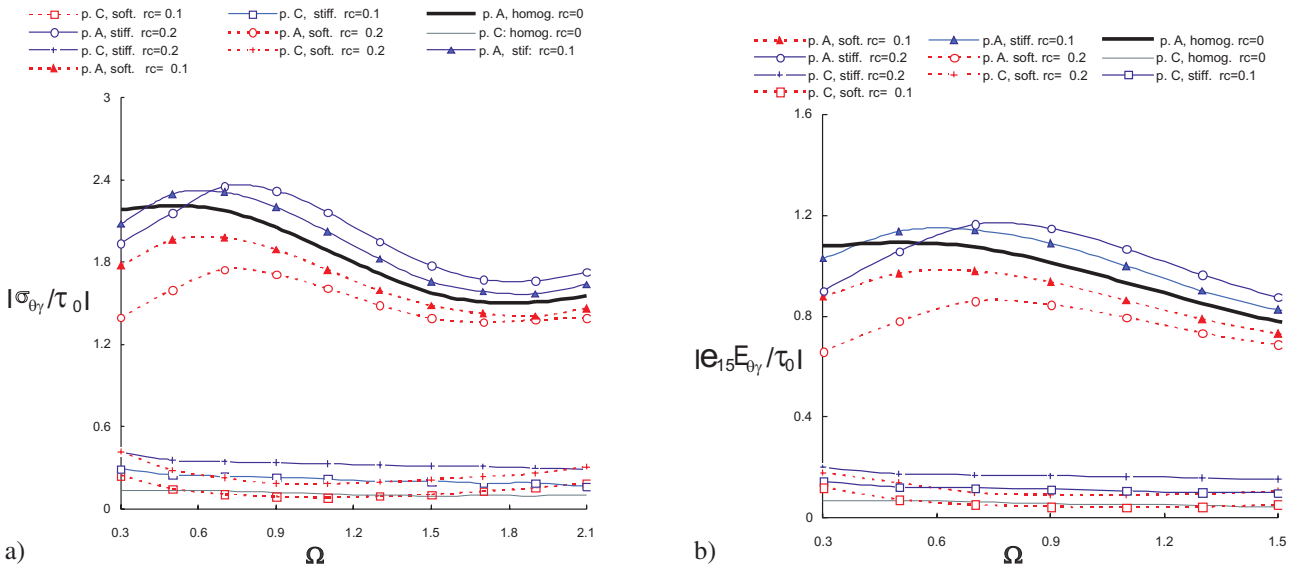

Fig. 6 (online colour at: www.zamm-journal.org) Dynamic GCF at observer points $A(0,c)$ and $C(c,0)$ versus normalized frequency Ω of the incident SH-wave with incident angle $\theta = 0$ at different inhomogeneity parameters rc and $\alpha = \pi/2, 3\pi/2$ for $E^* = 0$, i.e. pure mechanical load: (a) SCF; (b) EFCF.

the presence of inhomogeneity. Next, we see that the exponentially softening and stiffening inhomogeneous models yield different numerical values for dynamic stress and electric field concentrations. There is a shift of the maximum to the higher frequencies with increasing of the value rc. The SCFs and the EFCFs at observer $A(0,c)$ are much greater than at $C(c,0)$. The electro-mechanical coupling and dynamic overshooting phenomena are visible from these figures.

Figs. 7a,b describes analogous scenario like those in Figs. 6a,b but with the inhomogeneity direction $\alpha = 0$ or $\alpha = \pi$, i.e. along the Ox_1-axis. A comparison between results in Figs. 6, 7 show that the inhomogeneity effect is stronger when the inhomogeneity is along the Ox_2 axis, although even in the Figs. 7a,b the sensitivity of the stress and electric field concentrations to different stiffening and softening models can be seen. At $\Omega = 0.53$ the maximum of the curves shows the

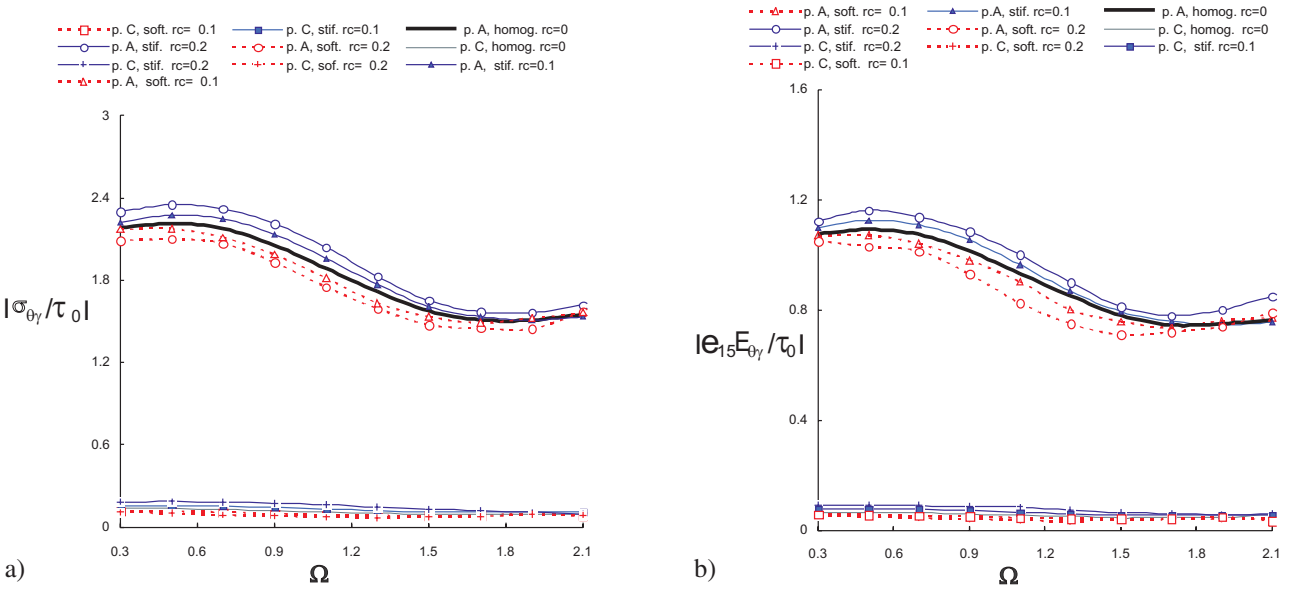

Fig. 7 (online colour at: www.zamm-journal.org) Dynamic GCF at observer points $A(0,c)$ and $C(c,0)$ versus normalized frequency Ω of the incident plane SH-wave with incident angle $\theta = 0$ for different inhomogeneity parameters rc and $\alpha = 0, \pi$ at $E^* = 0$, i.e. pure mechanical load: (a) SCF; (b) EFCF.

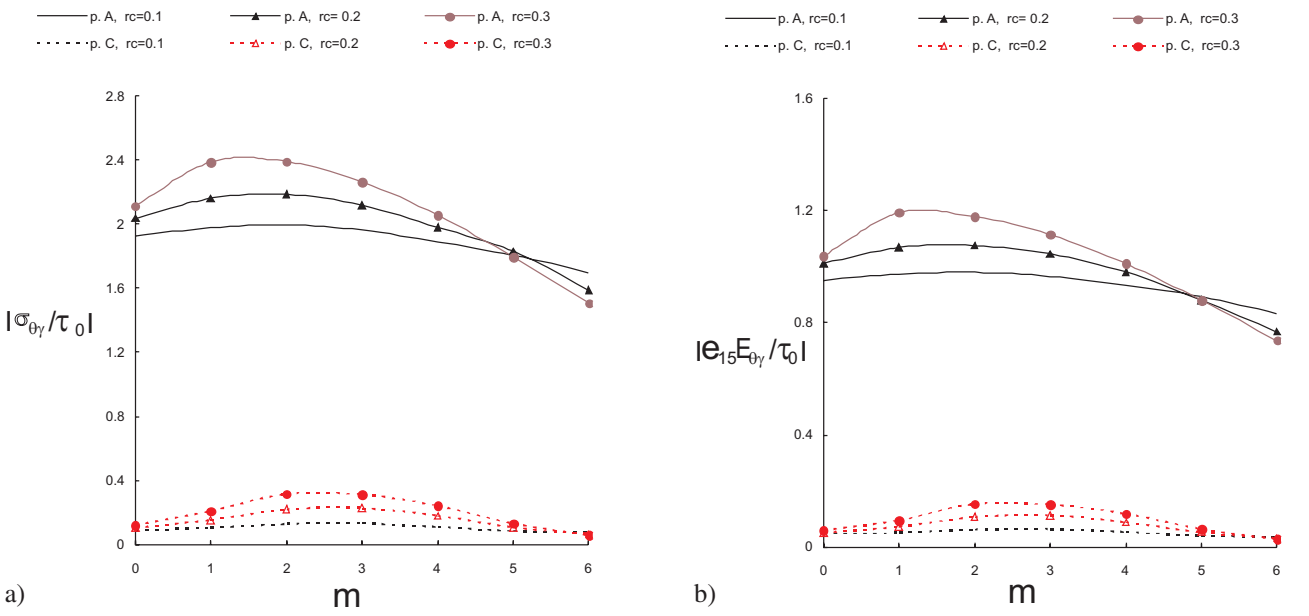

Fig. 8 (online colour at: www.zamm-journal.org) Dynamic GCF at observer points $A(0,c)$ and $C(c,0)$ versus inhomogeneity direction $\alpha = m\frac{\pi}{6}$ in the case of incident SH-wave with incident angle $\theta = 0$ for different inhomogeneity parameters rc, at for the normalized frequency $\Omega = 1.1$ and at $E^* = 0$, i.e. pure mechanical load: (a) SCF; (b) EFCF.

dynamic overshoot and this frequency is not shifted when the material inhomogeneity is involved, in contrast to the case when inhomogeneity direction is along Ox_2-axis, see Figs. 6a,b.

As far as the proposed methodology can take into consideration the lateral inhomogeneity, the sensitivity of the stress and electric field concentrations to the inhomogeneity direction can be seen in Figs. 8a,b, where the wave with a fixed frequency $\Omega = 1.1$ propagates along the Ox_1-axis and the inhomogeneity parameter is $rc = 0.1, 0.2, 0.3$. Figs. 9a,b are analogous but for the propagating wave along the Ox_2-axis. A comparison of the results in Figs. 8, 9 reveals that more sensitive to the direction of the material inhomogeneity are the cases when the wave propagates along the vertical axis

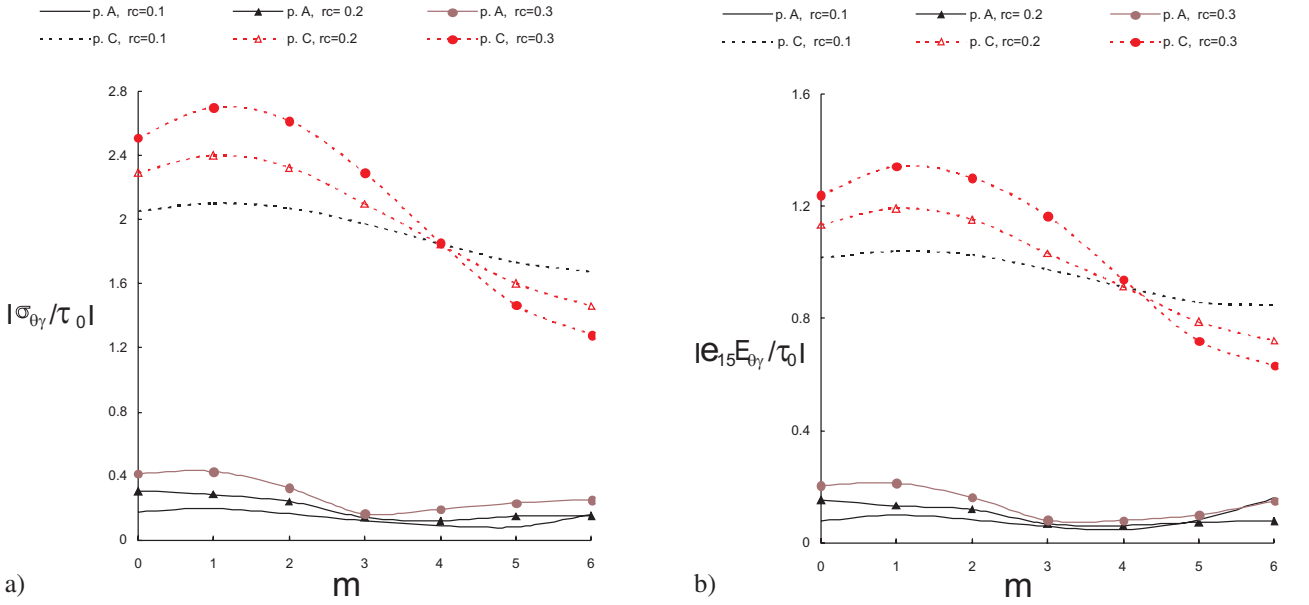

Fig. 9 (online colour at: www.zamm-journal.org) Dynamic GCF at observer points $A(0,c)$ and $C(c,0)$ versus inhomogeneity direction $\alpha = m\frac{\pi}{6}$ in the case of incident plane SH-wave with incident angle $\theta = \pi/2$ for different inhomogeneity parameters rc, at normalized frequency Ω and at $E^* = 0$, i.e. pure mechanical load: (a) SCF; (b) EFCF.

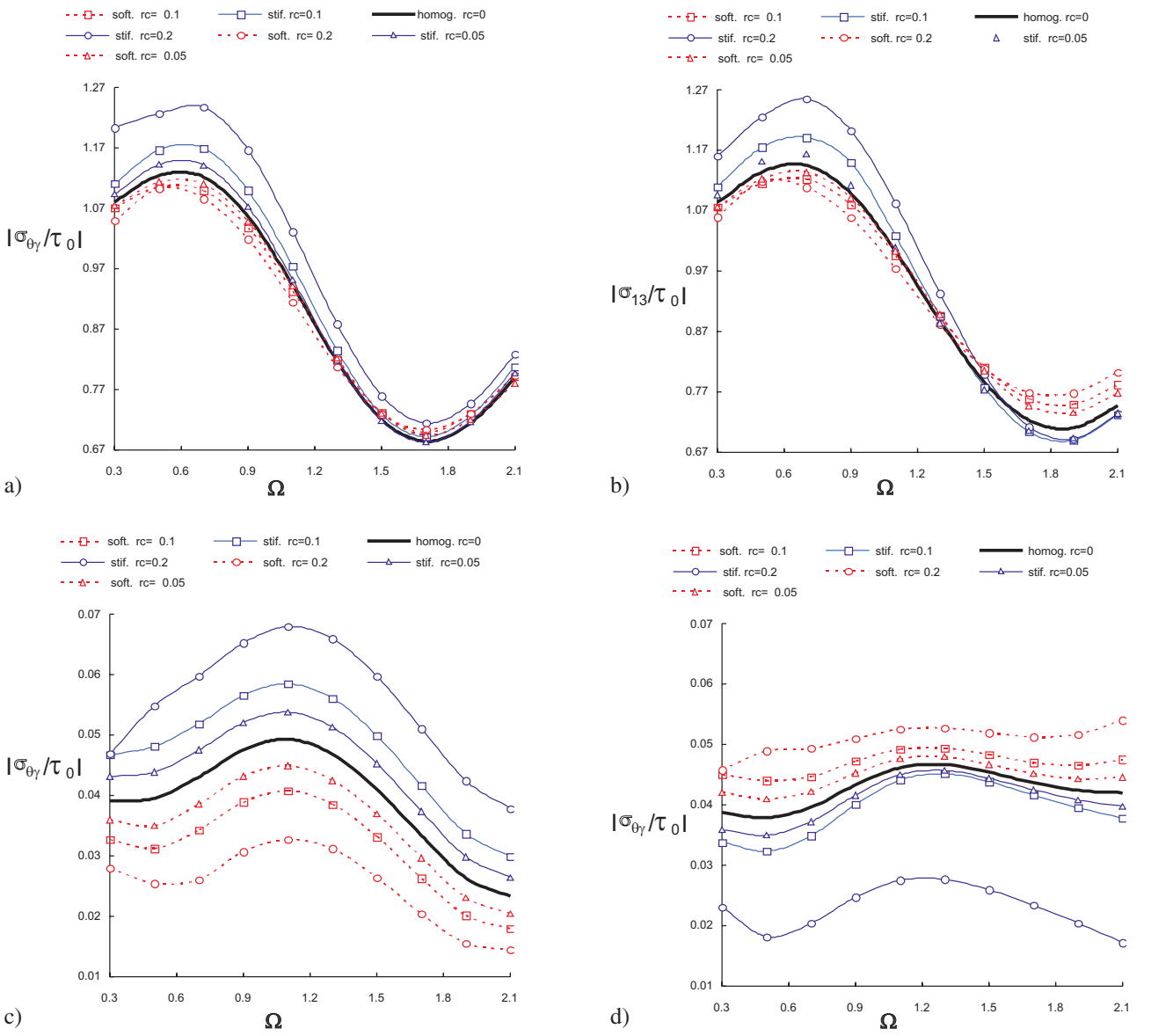

Fig. 10 (online colour at: www.zamm-journal.org) Dynamic SCF versus normalized frequency Ω of incident plane SH-wave with incident angle $\theta = 0$ for inhomogeneity direction $\alpha = 0$ (stiffening model) or $\alpha = \pi$ (softening model) at $E^* = 0.5$ and at observer points: (a) $A(0, c)$; (b) $B(0, -c)$; (c) $C(c, 0)$; (d) $D(-c, 0)$.

and when the inhomogeneous parameter rc is higher. Also, SCFs and EFCFs at point $A(0, c)$ are much greater than those at point $C(c, 0)$ in Figs. 8a,b. Conversely, the stress concentration is stronger at $C(c, 0$ than in $A(0, c)$ on Figs. 9a,b. The maximal values of SCFs and EFCFs are obtained for inhomogeneity direction in the interval $\alpha \in [\pi/3, 2\pi/3]$.

In order to measure the influence of the electric load on the generalized field of stress concentration near the hole, the results obtained at $E^* = 0.5$ are shown in Figs. 10, 11 at different values of the inhomogeneity parameter $rc = 0.05, 0.1, 0.2$. In Figs. 10, 11 the wave propagation direction and inhomogeneity direction are along Ox_1 axis. Figs. 10, 11 demonstrate convincingly that the dynamic stress and electric field concentrations can be considered as a complex result of different physical phenomena and their mutual internal interaction. These physical phenomena are: (a) wave-hole interaction; (b) wave-material interaction taking into consideration its anisotropy, inhomogeneity and electro-mechanical coupling that leads to the appearance and shifting of the resonance frequencies; (c) type and characteristics of the applied electromechanical load (pure mechanical, pure electrical and hybrid electro-mechanical); (d) coupled essence of the electro-mechanical nature of the piezoceramics. Due to the complex wave field around the hole the place of the observer where we measure the stress and electric field concentration is very important, compare Figs. 10a,b and Figs. 10c,d or Figs. 11a,b and

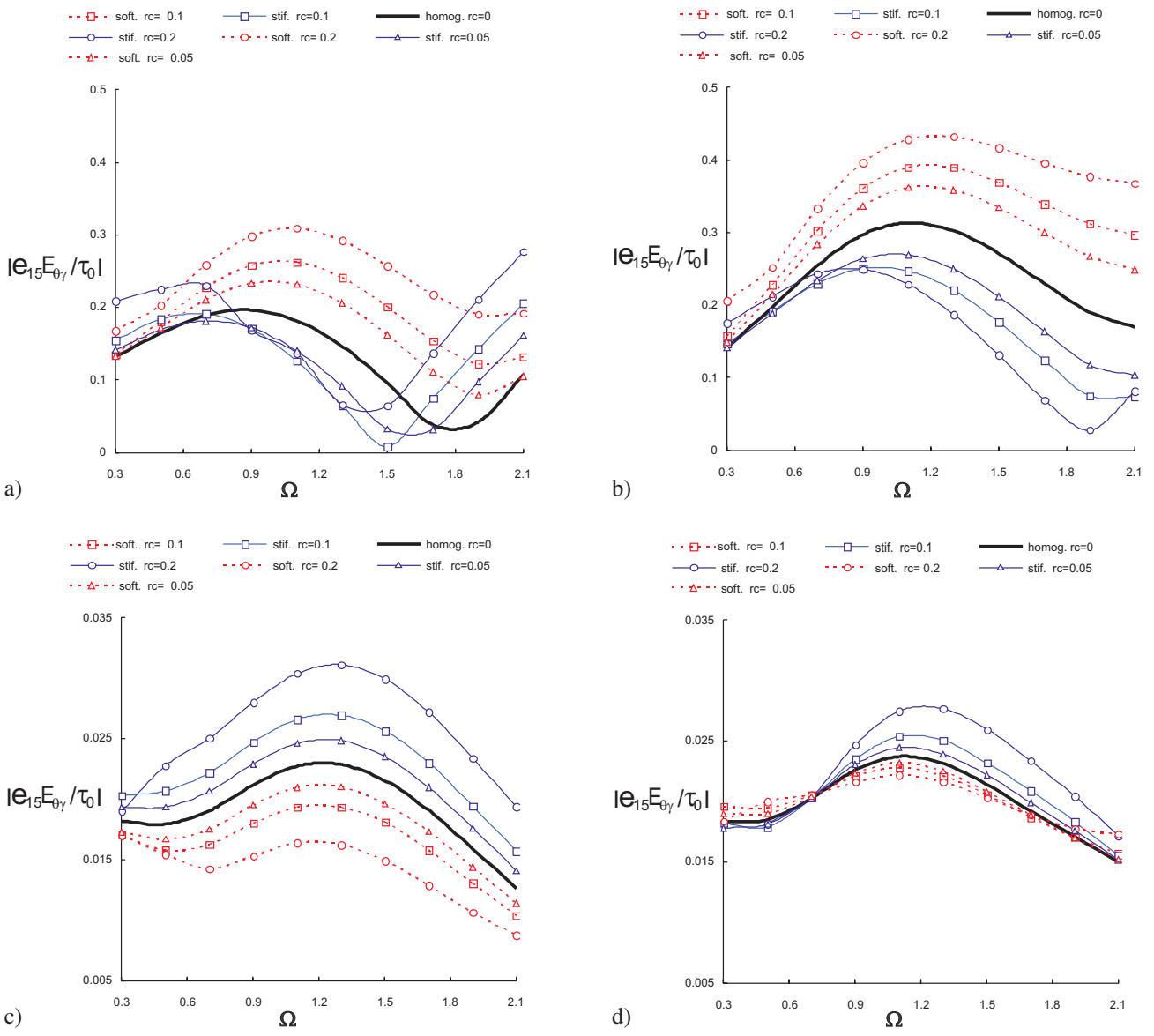

Fig. 11 (online colour at: www.zamm-journal.org) Dynamic EFCF versus normalized frequency Ω of incident plane SH-wave with incident angle $\theta = 0$ for inhomogeneity direction $\alpha = 0$ (stiffening model) or $\alpha = \pi$ (softening model) at $E^* = 0.5$ and at observer points: (a) $A(0, c)$; (b) $B(0, -c)$; (c) $C(c, 0)$; (d) $D(-c, 0)$.

Figs. 11c,d. It can be seen that the material inhomogeneity effect change the character of the SCF and EFCF curves for the cases of softening and stiffening material, see Fig. 10c and Fig. 11d. Note that this observer points are on the Ox_1-axis that in this case coincides with the material inhomogeneity direction.

It can be seen that the peak values of the dynamic stress and electric field concentration factor for functionally graded materials are different than that for the homogeneous material. So, the conclusion is that the defect driving force can be reduced by using the concept for the FGM and the idea to replace the homogeneous materials with smoothly inhomogeneous one in the new smart structure technologies works.

5 Conclusion

Two-dimensional dynamic anti-plane problem of a piezoelectric plane weakened with a circular hole is described by a system of non-hypersingular traction based BIEs. The numerical approach is based on the frequency dependent fundamental solution of the wave equation of exponentially inhomogeneous anisotropic piezoelectric material. The material properties vary exponentially with two spatial variables. The derivation of the fundamental solution is obtained by using an

appropriate algebraic transformation to the displacement vector and the properties of the Radon transform. The validated numerical scheme and the implemented software provides the electro-mechanical displacements along the hole boundary, the stress concentration factors near the hole and the scattered generalized displacement and traction in any point of the inhomogeneous piezoelectric plane.

The simulation results show conclusively that stress and electric field concentration near the hole in a functionally graded piezoelectric material is a complex result of the inter play of many key factors as: (a) the type of the material inhomogeneity and its magnitude and direction; (b) the type and properties of the electromechanical load; (c) the coupled nature of the electro-mechanical continuum; (d) the mutual disposition of the axis of material symmetry, the axis of material inhomogeneity, the polling axis, the wave polarization axis, and the direction of the wave propagation; (e) the location of the observer where the stress concentration factor is evaluated; (f) the relation between the inhomogeneity magnitude and the size of the hole.

The near-field results can be applied in computational fracture mechanics, while the information for the scattered wave field can be used for development of new efficient non-destructive test methods for monitoring the integrity and reliability of the multifunctional materials and smart structures based on them. The knowledge of the scattered wave field can be used as a basis for solution of inverse identification problems for the location and geometry of cracks. The proposed methodology can easily be extended to the problem of inclusions (one or more) in piezoelectric matrix with direct application to mechanics of composite materials and estimation of effective electromechanical properties in the case of randomly distributed inclusions.

Acknowledgements The authors acknowledge the support of the DFG under the grant number: 436BUL 113/150/0-1 and the support of the BNSF under the grant number: DID 02/15.

References

[1] M. Akamatsu and G. Nakamura, Well-posedness of initial-boundary value problems for piezoelectric equations, Applicable Analysis **81**, 129–141 (2002).
[2] H. Bateman and A. Erdelyi, Higher Transcendental Functions (McGraw-Hill, New York, 1953).
[3] M. L. Baron and A. T. Matthews, Diffraction of a pressure wave by a cylindrical cavity in an elastic medium, Trans. ASME, J. Appl. Mech. **28**, 347–354 (1961).
[4] M. L. Baron and R. Parnes, Displacements and velocities produced by the diffraction of a pressure wave by a cylindrical cavity in an elastic medium, Trans. ASME, J. Appl. Mech. **29**, 385–395 (1962).
[5] M. L. Baron and A. T. Matthews, Diffraction of a shear wave by a cylindrical cavity in an elastic medium, Trans. ASME, J. Appl. Mech. **29**, 205–207 (1962).
[6] M. Y. Chung and T. C. T. Ting, Piezoelectric solid with an elliptic inclusion or hole, Int. J. Solids Struct. **33**, 3343–3361 (1996).
[7] C. H. Daros, On modelling SH-waves in a class of inhomogeneous anisotropic media via the Boundary Element Method, Z. Angew. Math. Mech. **90**, 113–121 (2010).
[8] W. F. Deeg, The Analysis of Dislocation, Crack and Inclusion Problems in Piezoelectric Solids, (PhD thesis, Stanford University, CA, 1980).
[9] P. Dineva, D. Gross, and T. Rangelov, Dynamic interaction of cracks in piezoelectric and anisotropic solids: a non-hypersingular BIEM approach, Theor. Appl. Mech. (Belgrade) **35**(1–3), 73–91 (2008).
[10] P. Dineva and T. Rangelov, Time-harmonic behavior of a cracked inhomogeneous piezoelectric solid by BIEM, Theor. Appl. Mech. **39**(4), 93–100 (2009).
[11] P. Dineva, D. Gross, R. Müller, and T. Rangelov, Time-harmonic crack problems in functionally graded piezoelectric solids via BIEM, Eng. Fract. Mech. **77**, 73–91 (2010).
[12] A. C. Eringen and E. S. Suhubi, Elastodynamics, Vol. I and II (Academic Press, New York, 1974).
[13] X. Q. Fang, C. Hu, and S. Y. Du, Strain energy density of a circular cavity buried in a semi-infinite functionally graded materials subjected to shear waves, Theor. Appl. Fract. Mech. **46**, 166–174 (2006).
[14] X. Q. Fang, C. Hu, and W. H. Huang, Dynamic stress of a circular cavity buried in a semi-infinite functionally graded piezoelectric material subjected to shear waves, Eur. J. Mech. A, Solids **26**, 1016–1028 (2007).
[15] X. Q. Fang, Multiple scattering of electro-elastic waves from a buried cavity in a functionally graded piezoelectric material layer, Int. J. Solids Struct. **45**, 5716–5729 (2008).
[16] D. Gross, T. Rangelov, and P. Dineva, 2D Wave scattering by a crack in a piezoelectric plane using traction BIEM, Struct. Integr. Dur. **1**(1), 35–47 (2005).
[17] D. Gross, P. Dineva, and T. Rangelov, BIEM solution of piezoelectric cracked fnite solids under time-harmonic loading, Eng. Anal. Bound. Elem. **31**(2), 152–162 (2007).
[18] C. Hwu and C. Y. Liao, Special boundary element for the problems of multi-holes, cracks and inclusions, Comput. Struct. **51**(1), 23–31 (1994).
[19] C. P. Jiang, Z. H. Tong, and Y. K. Cheung, A generalized self-consistent method for piezoelectric fiber reinforced composites under antiplane shear, Mech. Mater. **33**, 295–308 (2001).
[20] G. Kirsch, Die Theorie der Elastizitat und die Bedürfnisse der Festigkeitslehre, VDI Z. **42**, 797–807 (1898).

[21] T. Kundu and A. Bostrom, Elastic wave scattering by a circular crack in a transversely isotropic solid, Wave Motion **15**, 285–300 (1992).
[22] V. Kupradze, Dynamical Problems in Elasticity. In: Progress in Solid Mechanics, Vol. 111, edited by N. Sneddon and R. Hill (North-Holland Publ. Comp., Amsterdam, 1963).
[23] J. S. Lee, Boundary element method for electroelastic interaction in piezoceramics, Eng. Anal. Bound. Elem. **15**(4), 321–328 (1995).
[24] V. W. Lee and M. D. Trifunac, Response of tunnels to incident SH waves, J. Eng. Mech. ASCE **105**, 643–659 (1979).
[25] D. Liu and H. Feng, The scattering of plane SH-waves by noncircular cavity in anisotropic media, Trans. ASME J. Appl. Mech. **60**, 769–772 (1993).
[26] Y. Liu and H. Fan, On the conventional boundary integral formulation for piezoelectric solidwith defects or thin shapes, Eng. Anal. Bound. Elem. **25**, 77–91 (2001).
[27] J. F. Lu and A. Hanyga, Dynamic interaction between multiple cracks and a circular hole swept by SH waves, Int. J. Solids Struct. **41**, 6725–6744 (2004).
[28] G. D. Manolis, Elastic wave scattering around cavities in inhomogeneous continua by the BEM, J. Sound Vibr. **226**(2), 281–305 (2003).
[29] J. Miklowicz, The Theory of Elastic Waves and Waveguides (North-Holland, Amsterdam, 1978).
[30] S. A. Meguid and Z. Zhong, On the elliptical inhomogeneity problem in piezoelectric materials under antiplane shear and inplane electric field, Int. J. Eng. Sci. **36**(3), 329–344 (1998).
[31] Y. E. Pak, Circular inclusion problem in antiplane piezoelectricity, Int. J. Solids Struct. **29**(19), 2403–2419 (1992).
[32] Y. E. Pak, Elliptical inclusion problem in antiplane piezoelectricity: implications for fracture mechanics, Int. J. Eng. Sci. **48**, 209–222 (2010).
[33] Y. H. Pao, Dynamic stress concentration in an elastic plate, J. Appl. Mech. **29**, 299–305 (1962).
[34] Y. H. Pao and C. C. Mow, Diffraction of Elastic Waves and Dynamic Stress Concentration (Crane Russak, NY, 1971).
[35] J. L. Perez-Aparicio, H. Sosa, and R. Palma, Numerical investigations of field-defect interactions in piezoelectric ceramics, Int. J. Solids Struct. **44**, 4892–4908 (2007).
[36] T. Rangelov, P. Dineva, and D. Gross, Effect of material inhomogeneity on the dynamic behavior of cracked piezoelectric solids: a BIEM approach, Z. Angew. Math. Mech. **88**, 86–99 (2008).
[37] T. Rangelov, P. Dineva, and D. Gross, On the influence of electric boundary conditions on dynamic SIFs in piezoelectric materials, in press, Arch. Appl. Mech. **80**, 985–996 (2010).
[38] G. N. Savin, Stress Concentration Around Holes (Pergamon Press, NY, 1961).
[39] Y. Shindo, H. Moribayashi, and F. Narita, Scattering of antiplane shear waves by a circular piezoelectric inclusion embedded in a piezoelectric medium subjected to a steady-state electrical load, Z. Angew. Math. Mech. **82**, 43–49 (2002).
[40] T. Song, H. Li, and J. Dong, Dynamic anti-plane behaviour of the interaction between a crack and a circular cavity in a piezoelectric medium, Key Eng. Mater. **324–325**, 29–32 (2006).
[41] H. Sosa, Plane problems in piezoelectric media with defects, Int. J. Solids Struct. **28**, 491–505 (1991).
[42] H. Sosa and N. Khutoryansky, New developments concerning piezoelectric materials with defects, Int. J. Solids Struct. **33**, 3399–3414 (1996).
[43] V. Vladimirov, Equations of Mathematical Physics (Nauka, Moskow, 1984).
[44] B. Wang, Three-dimensional analysis on an ellipsoidal inclusion in a piezoelectric material, Int. J. Solids Struct. **29**, 293–308 (1992).
[45] C.-Y. Wang and Ch. Zhang, 3-D and 2-D dynamic Green's functions and time-domain BIEs for piezoelectric solids. Eng. Anal. Bound. Elem. **29**, 454–465 (2005).
[46] X. L. Xu and R. K. N. D. Rajapakse, Boundary element analysis of piezoelectric solids with defects, Compos. B, Eng. **29**, 655–669 (1998).
[47] Ch. Zhang and D. Gross, On Wave Propagation in Elastic Solids with Cracks, (Computational Mechanics Publication, Southampton, 1998).
[48] A. Zayed, Handbook of Generalized Function Transformations (CRC Press, Boca Raton, Florida, 1996).

